

## Fluid flow and heat transport near the critical point of H<sub>2</sub>O

S.E. Ingebritsen

U.S. Geological Survey, Menlo Park, California

D.O. Hayba

U.S. Geological Survey, Reston, Virginia

**Abstract.** Near-critical extrema in the properties of water may influence flow patterns in hydrothermal systems, but singularities in equations of state for H<sub>2</sub>O at its critical point have inhibited quantitative modeling. Posing governing equations in terms of pressure ( $P$ ) and enthalpy ( $H$ ) avoids these singularities and facilitates computation. Numerical simulations with a  $P$ - $H$  based model show little near-critical enhancement in heat transfer for systems in which flow is driven by fixed pressure drops. However, in density-driven systems, near-critical variations in fluid properties can enhance convective heat transfer by a factor of 10<sup>2</sup> or more ("superconvection") if permeability is sufficiently high. Near-critical two-phase processes ("heat pipes") are at least equally effective at dissipating thermal energy. The restriction to high-permeability environments within a fairly narrow  $P$ - $H$  window suggests that superconvection may be quite rare in natural systems

### Introduction

The possible influence of near-critical phenomena on transport in hydrothermal systems has long been recognized. Near-critical variations in fluid properties tend to maximize buoyancy forces and heat-transport capacity while minimizing viscous-drag forces. Norton and Knight [1977] suggested that near-critical extrema in fluid properties may control the overall style of hydrothermal fluid circulation, while noting that small differential pressure and temperature ( $T$ ) values would be required to simulate the process adequately. Dunn and Hardee [1981] introduced the term "superconvection" to describe laboratory results that documented near-critical heat-transfer rates as much as 70 times greater than conductive rates.

The near-critical extrema in fluid properties create computational problems which have inhibited quantitative modeling, although Cox and Pruess [1990] attempted to reproduce the Dunn and Hardee results numerically. In the past, most users of geothermal models have had to choose between multiphase models with a temperature range of about 0-350 °C [e.g. Pruess, 1991] and models for single-phase, pure-water systems with a temperature range of about 0-1,000 °C

[e.g. Norton and Knight, 1977]. Both sets of models have tended to avoid the region very near the critical point.

For models that use pressure and temperature as dependent variables, the near-critical extrema pose particularly difficult problems. In  $P$ - $T$  coordinates, the critical point is at the vertex of the vaporization curve (Fig. 1A), and represents a singularity in equations of state. For example, the partial derivatives of density [ $\rho(P,T)$ ] diverge to  $\pm\infty$ , and heat capacity  $C_v(P,T)$  diverges to  $\infty$  [Johnson and Norton, 1991]. The HYDROTHERM model used in this study [Hayba and Ingebritsen, 1994] avoids computational problems at the critical point by formulating the governing equations in terms of pressure and enthalpy. In  $P$ - $H$  coordinates, two-phase conditions are represented as a region, rather than a single curve (Fig. 1B), and the density, viscosity, and temperature of liquid water and steam merge smoothly to finite values at the critical point (Fig. 1C). The  $P$ - $H$  formulation uniquely specifies the thermodynamic state of the fluid under both single- and two-phase conditions. HYDROTHERM is a descendent of subcritical codes developed at the U.S. Geological Survey in the late 1970's [Faust and Mercer, 1977; 1979a; 1979b]. Other  $P$ - $H$  and  $P$ -internal energy based multiphase models were developed at about the same time [cf. Voss, 1978] but were not applied to the near-critical problem.

### Mathematical approach

HYDROTHERM uses a finite-difference approach to simulate multiphase flow of pure water and heat at temperatures of 0-1,200 °C and pressures of 0.05-1,000 MPa. It solves the following expressions for mass and energy conservation:

$$\frac{\partial [n(S_w \rho_w + S_s \rho_s)]}{\partial t} - \nabla \cdot [k k_{rs} \rho_s / \mu_s \cdot (\nabla P - \rho_s g \nabla D)] - \nabla \cdot [k k_{rw} \rho_w / \mu_w \cdot (\nabla P - \rho_w g \nabla D)] - R_m = 0 \quad (1)$$

and

$$\frac{\partial [n S_w \rho_w H_w + n S_s \rho_s H_s + (1 - n) \rho_r H_r]}{\partial t} - \nabla \cdot [k k_{rs} \rho_s H_s / \mu_s \cdot (\nabla P - \rho_s g \nabla D)] - \nabla \cdot [k k_{rw} \rho_w H_w / \mu_w \cdot (\nabla P - \rho_w g \nabla D)] - \nabla \cdot K_m \nabla T - R_H = 0, \quad (2)$$

respectively, where  $n$  is porosity,  $S$  is volumetric saturation ( $S_w + S_s = 1$ ),  $\rho$  is density,  $t$  is time,  $k$  is intrinsic permeability,  $k_r$  is relative permeability ( $0 \leq k_r \leq 1$ ),  $\mu$  is dynamic viscosity,  $P$  is pressure,  $g$  is gravitational acceleration,  $D$  is depth,  $H$  is enthalpy,  $K_m$  is medium thermal conductivity,  $T$  is temperature,  $R_m$  and  $R_H$  are mass and energy source/sink flowrate terms, and the subscripts w, s, and r refer to liquid water, steam, and rock, respectively.

This paper is not subject to U.S. copyright. Published in 1994 by the American Geophysical Union.

Paper number 94GL02002

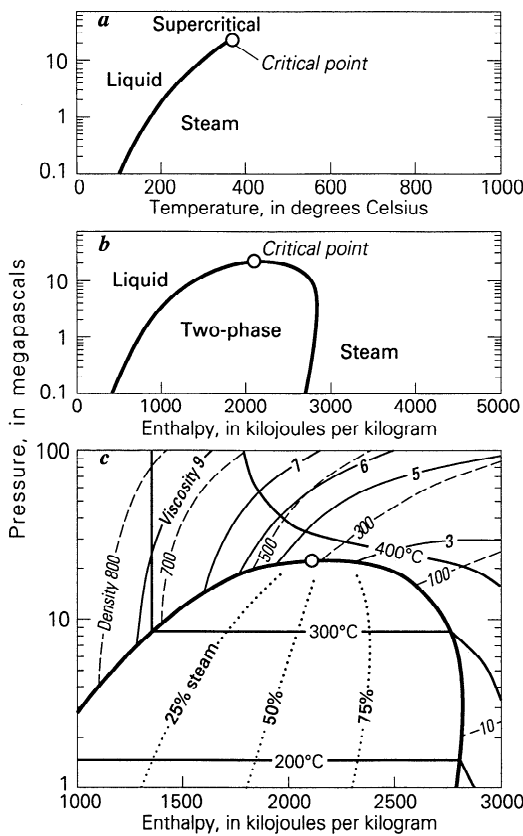


**Figure 1.** (A) Pressure-temperature and (B) pressure-enthalpy diagram, showing thermodynamic regions; (C), pressure-enthalpy diagram, showing contours of equal temperature (°C), density ( $\text{kg m}^{-3}$ ), viscosity ( $\text{Pa}\cdot\text{sec} \times 10^{-5}$ ), and mass fraction steam. Within the two-phase region the enthalpy of the fluid mixture,  $H_f$ , is calculated as  $[H_w S_w \rho_w + H_s S_s \rho_s] / [S_w \rho_w + S_s \rho_s]$ .

Assumptions implicit in these equations are that a two-phase form of Darcy's Law is valid; that rock and water are in thermal equilibrium; and that capillary-pressure effects and heat transfer by dispersion are negligible. Several constitutive relations complete the description of the system [Faust and Mercer, 1979a; Hayba and Ingebritsen, 1994]. A large (2 Mbyte) lookup table interrogated by a bicubic spline routine provides fluid densities, viscosities, and temperatures. We used fluid density and temperature values from the routines of Haar et al. [1984] and viscosity values from the formulation by Sengers and Watson [1986]. Cubic splines describe fluid properties at saturation. Each of the thermodynamic variables in equations (1) and (2) is finite at the critical point ( $P = 22.055 \text{ MPa}$ ,  $H = 2086.0 \text{ kJ kg}^{-1}$ ,  $T = 373.98 \text{ }^\circ\text{C}$ ,  $\rho = 322 \text{ kg m}^{-3}$ , and  $\mu = 3.94 \times 10^{-5} \text{ Pa}\cdot\text{s}$ ).

Equations (1) and (2) are strongly coupled and highly nonlinear, because a number of the independent variables are functions of the dependent variables  $P$  and  $H$ . HYDROTHERM uses Newton-Raphson iteration to treat the nonlinear coefficients. Mass and energy balances for each finite-difference block determine convergence. With the  $P$ - $H$  formulation, near-critical computations have actually proven to be less difficult than problems involving lower-pressure phase transitions, where there is a larger contrast in fluid properties.

Above the critical point, the distinction between liquid and steam disappears, and the values assigned to the saturation variables become arbitrary. To avoid problems in determining the average fluid properties for flow between super- and subcritical blocks, we treated supercritical blocks as though they contain two phases with identical properties.

**One-dimensional  $P$ - $H$  paths**

One-dimensional simulations indicate that permeability has a pivotal effect on near-critical  $P$ - $H$  trajectories. In a series of experiments, we modeled flow along a 1-km-long horizontal column, assigning various permeabilities and fixed  $P$ - $H$  values at the ends of the column. Equations (1) and (2) were solved iteratively until mass and energy fluxes reached a steady state. Thermal conductivity of the medium was held constant at  $2 \text{ W m}^{-1} \text{ K}^{-1}$ . Although there is some near-critical variation in the thermal conductivity of water, the resulting effect on  $K_m$  is small for low-porosity media, because  $K_m \sim K_r^{(1-n)} K_w^n$  [Sass et al., 1971].

Figures 2 and 3 show results from two sets of experiments with different  $P$ - $H$  endpoints. Within each set, differences in permeability cause the flow path to take different trajectories that are distinguishable in both  $P$ - $H$  (Fig. 2A) and  $P$ - $T$  (Fig. 2B) coordinates. In set 1, the high-permeability experiments intersect the critical point, and in set 2 the low-permeability runs do so.

At low permeabilities ( $\leq 10^{-18} \text{ m}^2$ ), heat transport by conduction dominates, and the  $P$ - $H$  and  $P$ - $T$  trajectories (Fig. 2) define a nearly constant temperature gradient (Fig. 3). At higher permeabilities ( $\geq 10^{-16} \text{ m}^2$ ), advection dominates, and the cooling trajectories reflect a nearly constant "flowing enthalpy", as defined by

$$(v_w \rho_w H_w + v_s \rho_s H_s) / (v_w \rho_w + v_s \rho_s), \quad (3)$$

where  $v$  is Darcian velocity (volumetric flowrate) (Fig. 3). Various quantitative analyses of flow near magmatic intru-

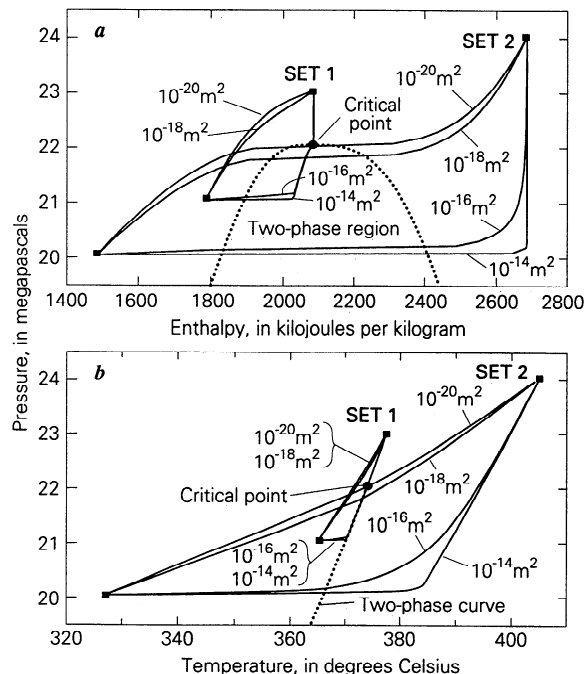


**Figure 2.** (A) Pressure-enthalpy and (B) pressure-temperature trajectories for two sets of one-dimensional experiments.

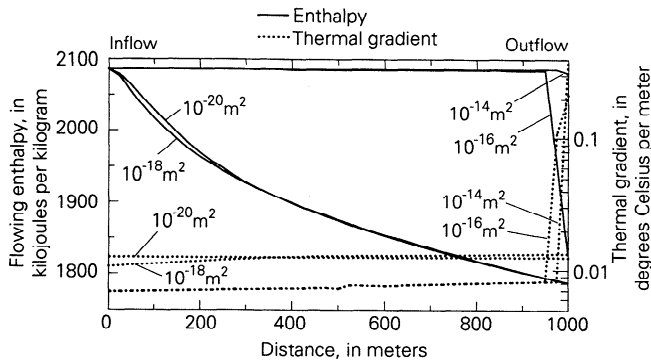


**Figure 3.** Results from experiment set 1 (Fig. 2), showing temperature gradient and flowing enthalpy as functions of distance along column.

sions have recognized a transition from conduction- to advection-dominated transport over the same permeability range [e.g. Norton and Knight, 1977].

In single-phase regions the "flowing enthalpy" is identical to the enthalpy of the *in situ* fluid, but in the two-phase region flowing enthalpy is strongly dependent on the mobilities of the two phases, and therefore on the choice of relative permeability functions. We used simple linear functions with no residual steam and liquid saturation to obtain the results shown here. Using different relative-permeability functions would change the trajectories of the high-permeability experiments through the two-phase region, but would not affect the transition from constant temperature gradient to constant flowing enthalpy over a finite range of permeabilities (Fig. 3).

Numerous subsequent one-dimensional experiments in which constant *P-H* boundaries were held much closer to the critical point showed little evidence of enhanced transport near the critical point; for particular endpoints, mass and energy fluxes scaled nearly linearly with permeability. Where flow is driven by a fixed pressure drop, near-critical phenomena appear to be much less important than variations in rock properties.

**Two-dimensional convection**

We used an equidimensional vertical slab to explore buoyancy driven flow. The upper and lower boundaries were impermeable and isothermal (with  $T_{bot} > T_{top}$ ), and the lateral boundaries were impermeable and insulated. Thermal conductivity was held constant at  $2.0 \text{ W m}^{-1} \text{ K}^{-1}$ . We varied the permeability of the slab ( $k$ ), the temperature drop across the slab ( $\Delta T$ ), the dimensions of the slab ( $\Delta L$ ), and initial pressure at the top of the slab ( $P_{top}$ ). The value of  $P_{top}$  was not held fixed, but the initial fluid density distribution was carefully prescribed to avoid thermal-pressurization effects, so that  $P_{top}$  did not vary greatly during the course of a simulation. Results are posed in terms of the Nusselt number,  $Nu$ , versus the average temperature of the slab ( $T_{ave}$ , or  $[T_{top} + T_{bot}]/2$ ). The Nusselt number is the ratio of the simulated heat-transfer rate to the purely conductive rate, or  $q/(K_m \Delta T/\Delta L)$ , where  $q$  is the horizontally averaged upward heat flux.

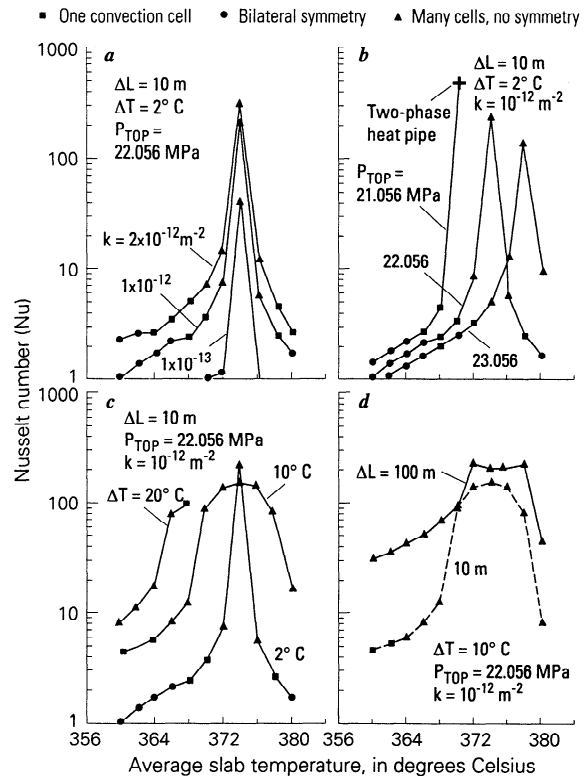
The two-dimensional experiments demonstrate "superconvection" driven by large near-critical density differences, and result in heat-transfer enhancement by factors of  $>10^2$ . Maximum  $Nu$  increases with permeability (Fig. 4A) and

shifts towards higher temperatures with increased  $P_{top}$  (Fig. 4B), following the fluid-property extrema, which also trend towards higher temperatures at pressures above the critical point. Results for larger  $\Delta T$  (Fig. 4C) and  $\Delta L$  (Fig. 4D) suggest that convection is strongly enhanced whenever the critical temperature lies within the slab (for example, for  $T_{ave}$  in the range of 370-378 °C for  $\Delta T = 10$  °C, and for  $T_{ave}$  in the range of 366-382 °C for  $\Delta T = 20$  °C). In convecting systems  $Nu$  is usually proportional to the Rayleigh Number  $Ra$ , and it has been noted previously that enhanced values of  $Ra$  can occur over a fairly broad near-critical *P-T* range [e.g. by Sengers, 1971].

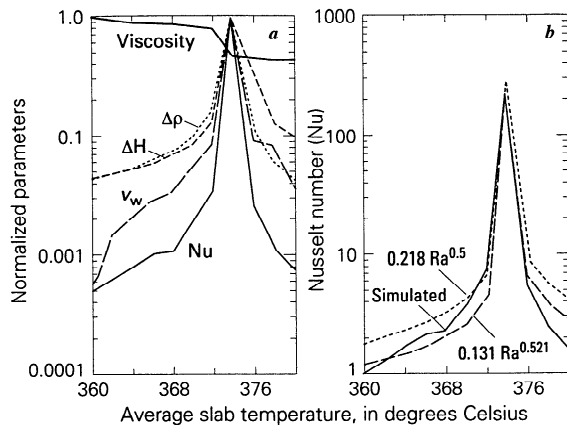
The complexity of convective flow increases with increasing  $Nu$ : there is a systematic variation from unicellular convection at  $Nu < 2.5$ , to bilaterally symmetric cells at  $Nu \sim 2.5-5$ , to numerous, smaller cells at  $Nu > 5$ .  $Nu \sim 5$  corresponds to  $Ra \sim 500$ , close to the suggested value for transition to unsteady flow [ $Ra \sim 400$ : Kimura et al., 1986].

Figure 5 shows additional results from the set of experiments at  $k = 10^{-12} \text{ m}^2$  shown in Figure 4A. Gradients in fluid enthalpy ( $H_{bot} - H_{top}$ , or  $\Delta H$ ) and density ( $\rho_{max} - \rho_{min}$ , or  $\Delta \rho$ ) across the slab both increase dramatically as  $T_{ave}$  approaches the critical temperature. The maximum fluid velocity ( $v_w$ ) in the slab is highly correlated with  $\Delta \rho$ , and  $Nu$  is highly correlated with the product of the mass flux and the enthalpy gradient ( $v_w \rho_w \Delta H$ ). Figure 5B shows that  $Nu$  is also proportional to the  $Ra$  value calculated using fluid properties at  $P_{top}$  and  $T_{ave}$ . The general correlation  $Nu = 0.218 Ra^{0.5}$  [Combarrous and Bories, 1975] fits our results fairly well, but a closer correlation is obtained by an empirical fit to our own results, which gives  $Nu = 0.131 Ra^{0.521}$ .

Nearly all of the two-dimensional results are single-phase, because  $P_{top}$  is .001 MPa or more greater than the critical



**Figure 4.**  $Nu$  as a function of  $T_{ave}$  for selected values of (A)  $k$ , (B)  $P_{top}$ , (C)  $\Delta T$ , and (D)  $\Delta L$ .



**Figure 5.** Further results from simulations with  $k = 10^{-12} \text{ m}^2$  summarized in Figure 4A. In (A), all parameters are normalized with respect to their maximum values ( $\Delta H = 406.5 \text{ kJ kg}^{-1}$ ,  $\Delta \rho = 226.3 \text{ kg m}^{-3}$ ,  $\mu = 6.48 \times 10^{-5} \text{ Pa-sec}$ ,  $v_w = 7.82 \times 10^{-6} \text{ m s}^{-1}$ , and  $Nu = 225$ ). In (B), our simulated  $Nu$  values are compared with  $Nu$  values calculated as  $f(Ra)$ .

pressure. Interestingly, the largest value of  $Nu$  belongs to the only two-phase result (Fig. 4B). In this case with  $P_{\text{top}} = 21.056 \text{ MPa}$ , a "heat pipe" occupies much of the slab: steam flows vertically upward and condenses, releasing latent heat of condensation near the top of the slab. An equivalent mass of liquid water percolates downward and vaporizes.

## Discussion

Our results show that near-critical variations in fluid properties can enhance convective heat transfer by a factor of  $10^2$  or more if permeability is sufficiently high. Near-critical two-phase processes seem to afford equally viable heat-transfer mechanisms, consistent with the fact that, for a given  $\Delta T$ ,  $\Delta H$  (in this case  $H_s - H_w$ ) and  $\Delta \rho$  ( $\rho_w - \rho_s$ ) are both larger under two-phase conditions than they can be at or above the critical point itself.

The permeability required for "superconvection" in our  $10\text{-m} \times 10\text{-m}$  slab with  $\Delta T = 2 \text{ }^\circ\text{C}$  is about  $10^{-13} \text{ m}^2$  (Fig. 4A), higher than is believed typical of near-magma environments. For example, the basaltic rocks that hosted the Skaergaard intrusion appear to have had time- and volume-averaged  $k \sim 10^{-16} \text{ m}^2$  [Manning *et al.*, 1993], and the hydrothermal systems of Kilauea's East Rift Zone are found in basalts with  $k \leq 10^{-15} \text{ m}^2$  [Ingebritsen and Scholl, 1993]. Simulations with dimensions and permeabilities more representative of a magmatic-hydrothermal system ( $\Delta L = 1 \text{ km}$ ,  $\Delta T = 100 \text{ }^\circ\text{C}$ ,  $P_{\text{top}} = 22.056 \text{ MPa}$ ,  $k = 10^{-16} - 10^{-15} \text{ m}^2$ ) led to  $Nu \leq 6$ . The restriction to high-permeability environments within a fairly narrow  $P$ - $T$  or  $P$ - $H$  window suggests that superconvection may be quite rare in natural systems. It may be most likely to occur where strain rates are sufficient to maintain permeability at depth despite competing processes such as silica deposition, for example, within high-angle fault zones in volcanic environments.

**Acknowledgments.** We thank Dina Lopez, Craig Manning, and Mike Sorey for helpful reviews.

## References

- Combarous, M.A., and S.A. Bories, Hydrothermal convection in saturated porous media, *Adv. Hydrosci.*, **10**, 231-307, 1975.
- Cox, B.L., and K. Pruess, Numerical experiments on convective heat transfer in water-saturated porous media at near-critical conditions, *Transp. in Porous Media*, **5**, 299-323, 1990.
- Dunn, J.C., and H.C. Hardee, Superconvecting geothermal zones, *J. Volcanol. and Geotherm. Res.*, **11**, 189-201, 1981.
- Faust, C.R., and J.W. Mercer, Finite-difference model of two-dimensional, single- and two-phase heat transport in a porous medium - Version I, *U.S. Geological Survey Open-File Rep.* 77-234, 84 pp., 1977.
- Faust, C.R., and J.W. Mercer, Geothermal reservoir simulation, 1, Mathematical models for liquid- and vapor-dominated hydrothermal systems, *Water Resour. Res.*, **15**, 23-30, 1979a.
- Faust, C.R., and J.W. Mercer, Geothermal reservoir simulation, 2, Numerical solution techniques for liquid- and vapor-dominated hydrothermal systems, *Water Resour. Res.*, **15**, 31-46, 1979b.
- Haar, Lester, J.S. Gallagher, and G.S. Kell, *NBS/NRC Steam Tables*, 320 pp., Hemisphere, New York, 1984.
- Hayba, D.O., and S.E. Ingebritsen, The computer model HYDROTHERM, a three-dimensional finite-difference model to simulate ground-water flow and heat transport in the temperature range of 0 to 1,200  $^\circ\text{C}$ , *U.S. Geological Survey Water-Resour. Invest. Rep.* 94-4045, 85 pp., 1994.
- Ingebritsen, S.E., and M.A. Scholl, The hydrogeology of Kilauea volcano, *Geothermics*, **22**, 255-270, 1993.
- Johnson, J.W., and Denis Norton, Critical phenomena in hydrothermal systems: State, thermodynamic, electrostatic, and transport properties of  $\text{H}_2\text{O}$  in the critical region, *Am. J. Sci.*, **291**, 541-648, 1991.
- Kimura, S., G. Schubert, and J.M. Straus, Route to chaos in porous-medium thermal convection, *J. Fluid Mech.* **166**, 305-324, 1986.
- Manning, C.E., S.E. Ingebritsen, and D.K. Bird, Missing mineral zones in contact metamorphosed basalts, *Am. J. Sci.*, **293**, 894-938, 1993.
- Norton, Denis, and J.E. Knight, Transport phenomena in hydrothermal systems: Cooling plutons, *Am. J. Sci.*, **277**, 937-981, 1977.
- Pruess, K., TOUGH2 - A general-purpose numerical simulator for multiphase fluid and heat flow, *Lawrence Berkeley Laboratory Rep. LBL-29400*, 102 pp., 1991.
- Sass, J.H., A.H. Lachenbruch, and R.J. Munroe, Thermal conductivity of rocks from measurements on fragments and its application to heat-flow determinations, *J. Geophys. Res.*, **76**, 3,391-3,401, 1971.
- Sengers, J.V., Transport properties of fluids near critical points in M.S. Green, ed., *Critical Phenomena*, pp. 445-507, Academic, New York, 1971.
- Sengers, J.V., and J.T.R. Watson, Improved international formulation for the viscosity and thermal conductivity of water substance, *J. Phys. Chem. Ref. Data*, **15**, 1,291-1,314, 1986.
- Voss, C.I., Finite element simulation of multiphase geothermal reservoirs, Ph.D. thesis, Princeton University, New Jersey, 1978.
- S.E. Ingebritsen, U.S. Geological Survey, 345 Middlefield Road, Menlo Park, CA 94025. (seingebr@rcamnl.wr.usgs.gov)
- D.O. Hayba, U.S. Geological Survey, 959 National Center, Reston, VA 22092. (dhayba@tonto.er.usgs.gov)

(Received June 16, 1994; accepted July 21, 1994)